Vol. 44 — N° 1 03 20 p. 125–132

GEOSTANDARDS and GEOANALYTICAL RESEARCH

Happy Jack Uraninite: A New Reference Material for High Spatial Resolution Analysis of U-Rich Matrices

Corinne **Dorais** (1)* , Antonio **Simonetti** (1), Loretta **Corcoran** (1), Tyler L. **Spano** (1) and Peter C. **Burns** (1, 2)

(1) Department of Civil and Environmental Engineering and Earth Sciences, University of Notre Dame, Notre Dame, IN, 46556, USA
(2) Department of Chemistry and Biochemistry, University of Notre Dame, Notre Dame, IN, 46556, USA
*Corresponding author. e-mail: cdorais@nd.edu

There is currently a lack of well-characterised matrix-matched reference materials (RMs) for forensic analysis of U-rich materials at high spatial resolution. This study reports a detailed characterisation of uraninite (nominally UO_{2+x}) from the Happy Jack Mine (UT, USA). The Happy Jack uraninite can be used as a RM for the determination of rare earth element (REE) mass fractions in nuclear materials, which provide critical information for source attribution purposes. This investigation includes powder X-ray diffraction (pXRD) data, as well as major, minor and trace element abundances determined using a variety of micro-analytical techniques. The chemical signature of the uraninite was investigated at the macro (cm)-scale with micro-X-ray fluorescence (μXRF) mapping and at high spatial resolution (tens of micrometre scale) using electron probe microanalysis (EPMA) and laser ablation-inductively coupled plasma-mass spectrometry (LA-ICP-MS) analyses. Based on EPMA results, the uraninite is characterised by homogeneous UO_2 and CaO contents of 91.57 ± 1.49% *m/m* (2*s* uncertainty) and 2.70 ± 0.38% *m/m* (2*s*), respectively. Therefore, CaO abundances were used as the internal standard when conducting LA-ICP-MS analyses. Overall, the major element and REE compositions are homogeneous at both the centimetre and micrometre scales, allowing this material to be used as a RM for high spatial resolution analysis of U-rich samples.

Keywords: reference material, LA-ICP-MS, uranium, high spatial resolution, rare earth elements.

Received 24 Jan 19 – Accepted 11 Jul 19

An essential component of global nuclear security is the prevention of the theft and trafficking of nuclear materials. To strengthen the protection of these materials, it is necessary to conduct a forensic investigation of the origin and trafficking pathway of recovered nuclear materials to remedy security weaknesses and prevent future thefts (Kristo *et al.* 2016). As part of such an investigation, researchers compare physical, chemical and isotopic characteristics of the interdicted material to a forensic database in an effort to identify possible source and trafficking routes (Moody *et al.* 2015). There is increasing evidence that one such chemical fingerprint, the relative mass fractions of rare earth elements (REEs), can be a useful nuclear forensic tool in determining the provenance of nuclear materials (e.g., Bürger *et al.* 2008, Keegan *et al.* 2008, Varga *et al.* 2010, Mercadier *et al.* 2011, Bürger *et al.* 2014, Kristo *et al.* 2016, Spano *et al.* 2017). The REEs, or lanthanides, are typically present as trace-level (ng g^{-1} to μg g^{-1}) constituents of raw uranium ores as well as processed uranium ore concentrates (UOCs). The relative mass fractions of these elements have been shown to be dependent on the geological environment in which the ore formed, allowing for the assignment of a particular deposit type based on the chondrite-normalised REE pattern.

Trace-level REEs are often measured via inductively coupled plasma-mass spectrometry (ICP-MS). Traditionally, these measurements have been made using solution mode (SM-) ICP-MS following sample preparation and digestion. However, Spano *et al.* (2017) recently demonstrated that the REE mass fractions within U ore and UOCs measured by laser ablation (LA-) ICP-MS are identical to those obtained via SM-ICP-MS. Although the former are associated with higher relative uncertainties compared to corresponding SM analyses, determination of the REE contents by LA-ICP-MS is a potentially powerful nuclear forensic tool (e.g., Krachler

doi: 10.1111/ggr.12293

et al. 2018). This is primarily because *in situ* analyses can be conducted much more quickly than SM analyses due to the ease of sample preparation. Additionally, LA-ICP-MS can provide vital information at high spatial resolution, which has the potential to identify chemical and/or isotopic heterogeneity that would be masked by bulk sample SM-ICP-MS analysis.

However, the versatility of the LA-ICP-MS method for nuclear forensic analysis is partially limited by a scarcity of high-quality, matrix-matched reference materials (RMs). Laser-based sampling techniques induce elemental fractionation, in part due to the interaction between the laser and the sample matrix (e.g., Günther and Hattendorf 2005). Although the extent of matrix-dependent fractionation can be reduced by optimising instrument parameters, reproducibility of quantitative measurements remains dependent on using RMs that match the sample matrix. For pre-detonation nuclear forensics, these RMs must be representative of nuclear materials, such as U ores and UOCs.

Uraninite ($(U_{1-x-y-z}^{4+}U_x^{6+}REE_y^{3+}M_z^{2+})O_{2+x-(0.5y)-z}$, Janeczek and Ewing 1992), which is the predominant U mineral in nature, may be well suited as a RM for *in situ* measurement of the REEs in UOCs and other nuclear materials; however, to date, few samples have been found that are both adequately homogeneous and available in sufficient quantities as to allow for distribution as a RM at the international level. The Mistamisk uraninite (Kish and Cuney 1981, Bonhoure *et al.* 2007) has been well characterised and previously presented as a RM for *in situ* analysis; however, we report here compositional heterogeneity within the uraninite matrix of this RM. Moreover, there is a lack of other suitable RMs for *in situ* analysis of U materials; additional RMs will allow for a more robust analytical capability. Furthermore, as the Mistamisk uraninite is a natural sample, there is a finite amount of material available for use and distribution to interested laboratories. Therefore, it is critical to develop additional uraninite RMs for *in situ* analysis. Ideally, such a RM will have a high, homogeneous content of UO_2 (≥ 90% *m/m*) with an equally homogeneous distribution of both the REEs and a minor element that can be used as an internal standard during LA-ICP-MS analyses.

The detailed chemical study of the Happy Jack (HJ) uraninite reported here is essential for nuclear forensic investigations because of the following reasons: (a) it is extremely important to fully characterise the starting material (natural U ores) in the nuclear fuel cycle in order to better understand chemical forensic signatures observed in subsequent, processed materials (e.g., UOCs); (b) the HJ uraninite is characterised by > 90% *m/m* UO_2, and therefore, it can be used to analyse UOCs as well as raw U ores; and (c) regardless of the degree of homogeneity of any unknown sample, high spatial resolution analysis requires the use of homogeneous standards, which renders the HJ uraninite investigated here valuable as a RM for *in situ* analysis of nuclear materials.

Experimental

For this work, a detailed chemical investigation of three hand specimens of uraninite totalling approximately 200 g (Figure 1) from the Happy Jack (HJ) Mine in White Canyon, UT (USA) was conducted in order to evaluate its potential as a RM for nuclear forensic applications. The host rock to the uranium mineralisation in White Canyon is the Shinarump conglomerate, which consists of feldspathic sandstones and conglomerates cemented together by calcite and silica (Trites and Chew 1955, Dahlkamp 1991). Of note, additional uraninite samples from other U deposits were investigated, but none found to be suitable for use as a RM; details are provided in the Appendix S1.

The crystalline structure of the HJ sample was confirmed using powder X-ray diffraction (pXRD). Data were collected using a Bruker Davinci automated diffractometer at room temperature over the angular range of 5–55° (2θ, CuKα) with a step width of 0.02° and a fixed counting time of 20 s/step.

Small pieces of uraninite were cut from each of the three hand specimens and placed in 1-inch-diameter epoxy mounts before being polished in preparation for *in situ* analysis. The cm-scale homogeneity of the major elements was investigated using micro-X-ray fluorescence (μXRF) elemental mapping, which provided a qualitative measure of the spatial distribution of elements comprising ≥ 1% *m/m* of the sample.

The polished epoxy mounts were carbon-coated prior to *in situ* electron probe microanalysis (EPMA). A Cameca SX-50 electron microprobe was used to quantitatively determine major and minor oxide compositions as well as to establish an internal standard for use with LA-ICP-MS. Analyses were conducted using an accelerating voltage of 15 kV along with a beam size of 15 μm and a beam current of 100 nA. Prior to analysis of unknowns, standardisation was performed using well-characterised standards of synthetic uranium dioxide (UO_2), galena (PbS), synthetic thorium dioxide (ThO_2), synthetic zircon ($ZrSiO_4$), anorthite-composition glass ($CaAl_2Si_2O_8$), titanium dioxide (TiO_2), Mn metal, synthetic Y-Al garnet ($Y_3Al_5O_{12}$), synthetic calcium

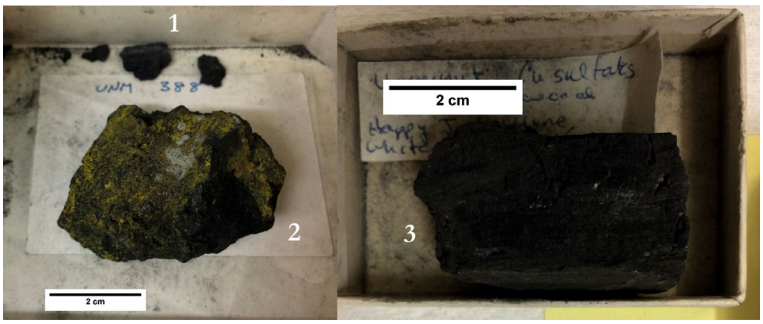

Figure 1. The Happy Jack uraninite is composed of three separate hand specimens: small black piece (1), a large piece with an alteration rind (2) and a large black piece (3). In total, the sample weighs approximately 200 g. [Colour figure can be viewed at wileyonlinelibrary.com]

phosphide (Ca_2P), synthetic vanadium oxide (V_2O_3), K-feldspar, Mn-bearing olivine ($(Mg^{2+}, Fe^{2+})_2SiO_4$) and arsenic. Corrections were made according to the Pouchou and Pichoir method (1991); uncertainties (2*s* mean) were calculated from counting statistics. A total of fifty-six spots were analysed across the three mounts.

In situ trace element compositions were obtained by LA-ICP-MS using a New Wave Research UP213 Nd:YAG laser system coupled to a Thermo Scientific Element 2 high-resolution (HR-) ICP-MS. Prior to analysis, background signals were measured for 60 s with the laser on and shuttered. Ablation spot size was 30 μm with a 5 Hz repetition rate, resulting in pits approximately 50 μm deep (e.g., Schurr *et al.* 2018). Analyses were conducted using the calibrator-sample bracketing method, employing the NIST SRM 610 glass (Pearce *et al.* 1997) as the reference material. Calcium (determined by EPMA) was used as the internal standard element to monitor instrumental drift. Data reduction was performed using Glitter software (van Achterbergh *et al.* 2001), which determines mass fractions, internal uncertainties and limits of detection. Mass fractions of the REEs were normalised to chondritic abundances (McDonough and Sun 1995). Mounted samples of each hand specimen were analysed for a total of forty-seven spots across three mounts. The instrument parameters and operational settings are located within the Appendix S1 section.

Locations for both EPMA and LA-ICP-MS analyses were chosen to be representative of the entire surface of the mounted sample. *In situ* analyses were also conducted on a piece of the Mistamisk uraninite (Kish and Cuney 1981, Bonhoure *et al.* 2007). The Mistamisk uraninite has been extensively characterised, and therefore, the major and trace element compositions of the HJ uraninite are compared with that of the Mistamisk uraninite to allow for a metric of homogeneity.

In order to establish the HJ uraninite as a RM for *in situ* work, it is imperative to determine its bulk chemical composition in order to serve as a comparison with the LA-ICP-MS results and verify its macro-scale homogeneity. Therefore, representative fragments were taken from each of the three hand specimens and digested in 15-ml perfluoroalkoxy (PFA) capped beakers using double-distilled HNO_3 and HF at 120 °C in a class 1000 clean room before being prepared in duplicate using the spike addition method (after Jenner *et al.* 1990). Solution mode ICP-MS analyses were conducted on a Nu Instruments Attom HR-ICP-MS in medium mass resolution; instrument and operation settings are listed in the Appendix S1.

For a more complete characterisation of the HJ uraninite, U isotope measurements were also carried out. Prior to analysis, aliquots of the digested material were processed through UTEVA exchange columns to purify the U and remove potential interferences (Pollington *et al.* 2016). Isotope ratio measurements were conducted using a Nu Instruments Nu Plasma II multi-collector (MC)-ICP-MS. Duplicates of each digestion were run using sample-standard bracketing with CRM 112-A (New Brunswick Laboratory 2010) as the external standard. Reported associated uncertainties (2*s* level) are based on the average values obtained across all three hand specimens. MC-ICP-MS instrument and operation settings can be found in the Appendix S1.

Results and discussion

The fluorite structure of the Happy Jack uraninite was confirmed by pXRD (Figure 2). Secondary, minor mineral phases observed include SiO_2- and Cu-Fe-S-rich phases. These inclusions are readily apparent during *in situ* work as they have physical appearances that are distinct from the uraninite matrix, and may be avoided during *in situ* analysis

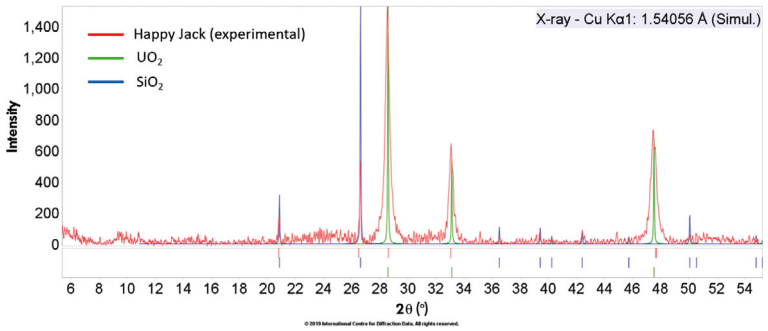

Figure 2. The pXRD pattern confirms the fluorite structure of the Happy Jack uraninite with minor inclusions of compositionally distinct secondary phases (e.g., SiO_2, shown here). [Colour figure can be viewed at wileyonlinelibrary.com]

(Figure 3). Secondary phases are also apparent in elemental maps (Figure 4), which were created from qualitative mass fraction measurements of elements present at or above ~ 1% *m/m* as determined by μXRF. The elemental maps also illustrate the homogeneous distribution of U and Ca in the uraninite matrix at the macro (cm)-scale. Additional BSE images and μXRF elemental maps are included in the Appendix S1.

As the HJ uraninite is a natural sample, individual subsamples will contain varying amounts of minor alteration and secondary mineralisation. Secondary mineral inclusions range in size from several μm to several mm and are concentrated in highly fractured areas. Therefore, it is recommended that researchers wishing to adopt the HJ uraninite as a RM first use a robust, semi-quantitative method such as μXRF to assess and identify the spatial distribution of any secondary phases contained within their allotted fragment. Such characterisation will not identify secondary phases present at depth, which may inadvertently be ablated; however, REE mass fractions differ significantly between the uraninite matrix and associated alteration minerals (e.g., Balboni *et al.* 2017). Consequently, if a subsurface inclusion is ablated, then these can be easily identified and omitted in the time-resolved laser ablation profiles for individual analyses.

Major and minor oxide mass fractions for UO_2 (91.57 ± 1.49% *m/m*, 2*s* uncertainty) and CaO (2.70 ± 0.38% *m/m*, 2*s* uncertainty) were determined using EPMA (Table 1). Other elements (Al, Si, P, S, K, Ti, V, Mn, Fe, As, Y, Zr, Pb and Th) were present at low values and therefore not quantifiable at high precision by EPMA. However, they have been included in Table 1 for comparative purposes. Calcium was chosen as the internal standard for LA-ICP-MS because of its homogeneous distribution and its abundance at an appropriate level. Additionally, Ca is an appropriate internal standard as it is ablated and ionised with approximately the same efficiency as both U and the REEs (e.g., Fryer *et al.* 1995).

Chondrite-normalised (CN-) REE mass fractions were determined by LA-ICP-MS (Table 2). The CN-REE pattern is characterised by a depletion in La (fifty-eight times chondrite) followed by a slight increase in the mid-light REEs (Ce-Sm) and a relatively flat pattern for the remaining REEs at levels approximately 1300 times chondrite (Figure 5). The mass fractions of the lanthanides are fairly homogeneous, although there is relatively more variation in the light REE abundances.

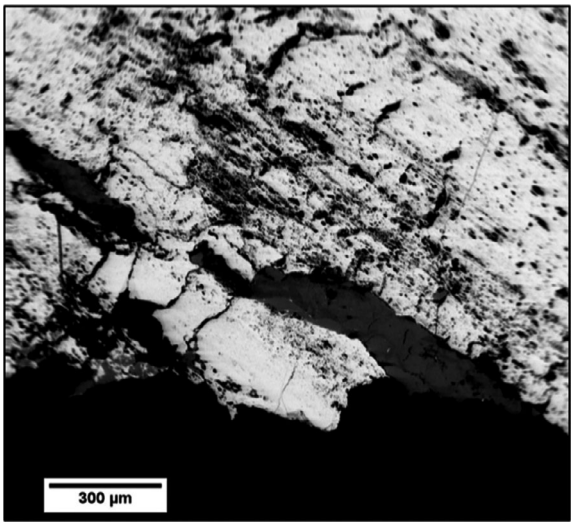

Figure 3. BSE image of a section of HJ uraninite exhibiting minor mineral phases rich in Cu, Fe and S (dark grey area), which are easily distinguished from the UO_2 matrix (light grey region).

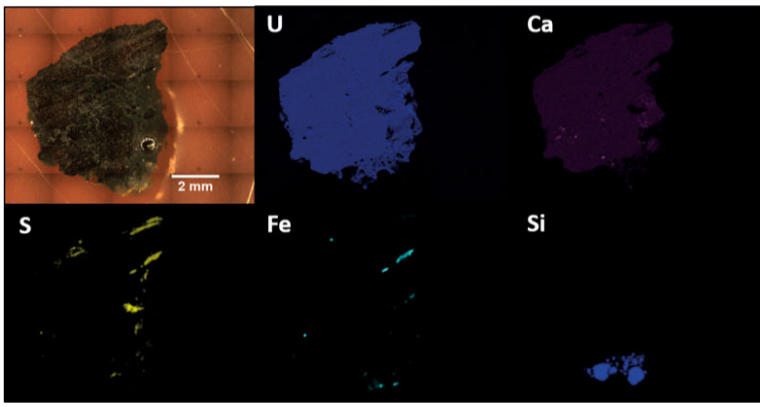

Figure 4. Elemental maps of section 1 of the HJ uraninite generated by μXRF demonstrate the macro-scale homogeneity of the sample with respect to U and Ca. Minor inclusions of secondary mineral phases can be observed in the Ca-rich areas as well as in areas where S, Fe and Si are present. [Colour figure can be viewed at wileyonlinelibrary.com]

Table 1.
Mean mass fractions (% *m*/*m*) of UO_2 and CaO are within uncertainty (2*s*) across all three sections of the HJ uraninite

	Mean	Uncert	1	Uncert	2	Uncert	3	Uncert
UO_2	91.57	1.49	91.90	1.41	91.20	1.29	91.61	1.47
CaO	2.70	0.38	2.82	0.30	2.59	0.37	2.66	0.33
FeO	0.47	0.34	0.39	0.26	0.58	0.54	0.48	0.37
PbO	0.42	0.42	0.32	0.29	0.49	0.44	0.48	0.44
SiO_2	0.39	0.33	0.33	0.20	0.46	0.37	0.40	0.38
V_2O_3	0.37	0.10	0.35	0.08	0.39	0.08	0.37	0.11
P_2O_5	0.36	0.10	0.37	0.11	0.35	0.09	0.38	0.10
K_2O	0.21	0.02	0.21	0.01	0.20	0.02	0.20	0.02
Y_2O_3	0.19	0.06	0.18	0.05	0.21	0.05	0.17	0.07
ZrO_2	0.13	0.17	0.08	0.07	0.22	0.07	0.08	0.13
TiO_2	0.12	0.30	0.10	0.13	0.10	0.09	0.17	0.58
SO_3	0.08	0.22	0.10	0.27	0.17	1.25	0.09	0.20
MnO	0.05	0.08	0.03	0.05	0.06	0.08	0.07	0.08
Al_2O_3	0.04	0.04	0.03	0.02	0.04	0.05	0.05	0.05
As_2O_3	0.01	0.02	0.01	0.02	0.01	0.02	0.01	0.02
ThO_2	0.01	0.02	0.01	0.02	0.01	0.01	0.01	0.02
Sum	97.12	1.61	97.24	1.39	96.86	1.77	97.22	1.72

To minimise associated uncertainties, means may be taken for each of the sections independently. Other elements measured via EPMA were not present in high enough mass fractions to measure with precision, but are included here for comparative value.

Table 2.
Mean REE mass fractions (μg g^{-1}) were determined for the HJ uraninite across all three sections as well as for each individual section

	Average	Uncert.	1	Uncert.	2	Uncert.	3	Uncert.
La	21.5	14.1	18.1	12.3	26.4	12.7	21.1	12.2
Ce	1203	524	1044	438	1372	467	1279	407
Pr	288	82.6	263	70.1	316	75.5	296	58.5
Nd	1533	356	1426	307	1646	324	1581	252
Sm	403	85.2	372	61.1	448	52.0	400	42.2
Eu	129	18.8	124	17.7	136	14.4	132	12.1
Gd	83.4	15.6	77.9	11.1	92.2	8.2	81.8	7.0
Tb	394	75.5	369	55.5	436	42.8	386	38.7
Dy	559	103	520	67.8	618	50.7	551	44.8
Ho	111	20.3	104	13.5	123	9.48	110	9.58
Er	308	56.1	289	38.4	341	27.3	302	28.0
Tm	48.2	8.78	45.1	5.68	53.3	4.09	47.0	4.41
Yb	363	58.7	345	40.2	397	28.7	351	31.0
Lu	36.9	8.04	33.6	3.99	41.8	3.53	36.4	3.68

Although the values are all within uncertainty (2*s*), uncertainties can be minimised by using an individual section mass fraction for a given mount.

The individual mean mass fractions for each of the three hand specimens are identical (within their respective uncertainties) for both the major and minor oxide compositions as well as REE mass fractions. However, because the HJ uraninite is a natural sample, there is some spatial, inter-sample variation. This is evident in the lower uncertainties associated with the average compositions for an individual sample piece relative to the slightly higher uncertainties associated with the global average, as reported in Tables 1 and 2. Therefore, in order to minimise the uncertainties associated with the U, Ca and REE mass fractions, it is recommended that similar *in situ* analyses be conducted on an individual subsample prior to its use as a RM for LA-ICP-MS investigation.

Although the uncertainties associated with both oxide and REE mass fractions are higher than in a manufactured RM such as a NIST glass, the HJ uraninite is more homogeneous than compositions previously reported for U-rich natural materials. For example, in Figure 6, the CaO %

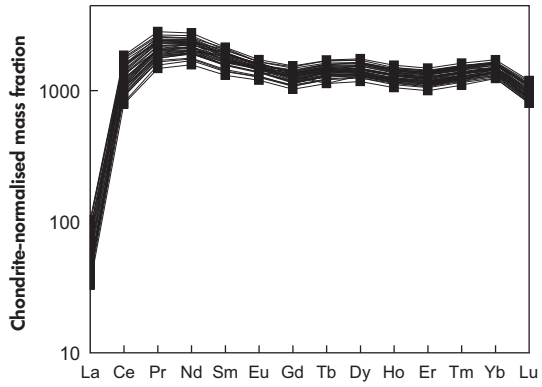

Figure 5. Chondrite-normalised REE patterns for the HJ uraninite as determined by LA-ICP-MS. The pattern is well constrained for all analyses (*n* = 47), indicating a high level of homogeneity.

m/m abundances and CN-REE abundances for the HJ uraninite are compared to the well-characterised Mistamisk uraninite; as illustrated in Figure 6, both Ca and the REE contents are less variable in the HJ uraninite than in the Mistamisk uraninite, indicating a higher level of homogeneity.

To validate the *in situ* REE mass fractions obtained for the HJ uraninite, digestions of each hand specimen were analysed via SM-ICP-MS. The CN-REE patterns based on the SM-ICP-MS analyses are in good agreement with their LA-ICP-MS derived counterparts (Figure 7); however, mass fractions for the mid-heavy REEs are slightly lower than those obtained via LA-ICP-MS (see Table 3). This is likely due to the inclusion and digestion of minor mineral phases, which were observed during *in situ* analysis. As illustrated in Figure 3, these Cu-Fe-S-rich phases are readily identifiable in back scattered electron (BSE) imaging due to their low atomic mass compared to the dominant uraninite. Therefore, these were easily excluded during *in situ* analyses. However, because the Cu-Fe-S phases are expected to incorporate fewer REEs (George *et al.,* 2018), their dissolution during bulk sample digestion effectively dilutes the total abundance of REEs recorded in the SM analyses. Although the REEs are the only trace elements found to be homogeneous across all three hand specimens, within a single sample mount, there may be more homogeneous mass fractions for certain trace elements that allow for additional quantification. For example, the overall mean Y mass fraction for all three specimens is 1504.8 ± 416.6 μg g^{-1}; however, the Y mass fractions for samples 1, 2 and 3 are 1353.0 ± 271.7, 1450.2 ± 174.0 and 1757.3 ± 147.1 μg g^{-1}, respectively.

The $^{238}U/^{235}U$ and $^{234}U/^{235}U$ isotope compositions for the HJ uraninite averaged across all three hand specimens

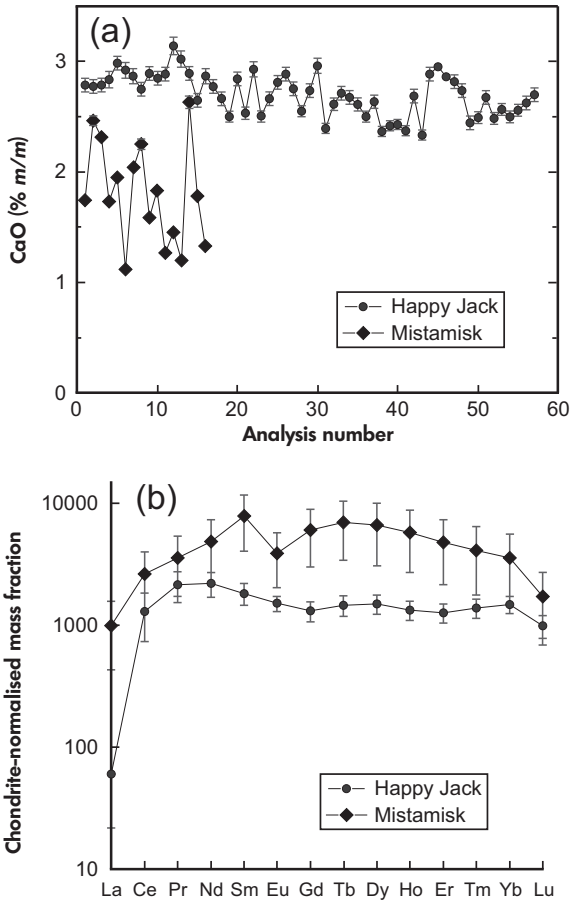

Figure 6. The distributions of (a) CaO (% *m/m*) and (b) REE abundances for the HJ uraninite are compared with the respective distributions in the Mistamisk uraninite (Kish and Cuney 1981, Bonhoure *et al.* 2007) obtained here. Both Ca and the REE contents are less variable in the HJ uraninite than in the Mistamisk uraninite, indicating more homogeneously distributed mass fractions. Uncertainties are at 2*s* level (a), or represent the range of values observed (b).

are 0.00724 ± 0.00001 (2*s*) and 0.00762 ± 0.0003 (2*s*), respectively. This is consistent with values previously reported for uraninite (e.g., Hiess *et al.,* 2012, Spano *et al.* 2017).

Conclusions

The HJ uraninite described herein is suitable as a RM for *in situ* analysis of U-rich materials, including raw U ores and UOCs. It is characterised by a homogeneous composition relative to both UO_2 (91.57 ± 1.49% *m/m*) and CaO (2.70 ± 0.38% *m/m*) abundances, the latter of which can be used as an internal standard to correct for instrumental drift during LA-ICP-MS analysis. The REEs are homogeneously distributed throughout the sample at abundances

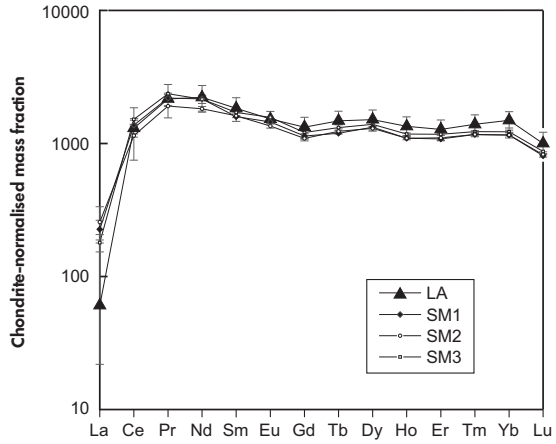

Figure 7. REE mass fractions obtained by both SM- and LA-ICP-MS analyses are overall in good agreement.

Table 3.
The mean SM-ICP-MS REE mass fractions (μg g^{-1}) are within uncertainties across digested aliquots

1	Uncert.	2	Uncert.	3	Uncert.
85.1	14.3	96.6	29.3	67.6	10.0
1310	22	1098	29	1451	20
301	1.83	262	2.05	324	3.62
1532	111	1295	52.5	1526	37.8
367	5.58	372	3.11	395	4.26
126	3.25	117	4.36	137	0.12
348	14.3	334	14.0	369	26.1
69.2	0.25	71.4	3.21	76.4	3.73
505	5.50	494	13.5	530	19.4
92.8	0.02	93.3	2.72	99.8	2.32
269	6.72	274	12.7	292	5.23
41.4	0.83	41.7	1.74	43.7	0.53
287	13.8	285	12.8	303	20.8
30.8	0.69	31.4	0.56	33.1	0.16

~ 1300 times chondrite with the exception of La (approximately sixty times chondrite). Used in conjunction with a certified RM, such as a NIST glass, the HJ uraninite may allow for more accurate *in situ* measurement of REE mass fractions in natural uranium materials as it will be matrix-matched to samples of interest.

Acknowledgements

The authors thank Dr. Ian Steele for his generous assistance with EPMA analyses, Dr. Enrica Balboni for her assistance with preliminary sample identification, the University of Notre Dame Center for Environmental Science and Technology (CEST) for the use of the μXRF, and ND Energy's Materials Characterisation Facility for access to EPMA. The HJ uraninite was obtained from the Rod Ewing Mineral Collection, housed at the University of Notre Dame. Funding for this work was provided by the United States Department of Homeland Security grant DHS-14-DN-077-ARI-001.

References

van Achterbergh E., Ryan C.G., Jackson S. and Griffin W.L. (2001)
Data reduction software for LA-ICP-MS. In: Sylvester P. (ed.), Laser-ablation-ICP-MS in the earth sciences principles and applications. Mineralogical Association of Canada (Ottawa, ON).

Balboni E., Simonetti A., Spano T., Cook N.D. and Burns P.C. (2017)
Rare-earth element fractionation in uranium ore and its U (VI) alteration minerals. Applied Geochemistry, 87, 84–92.

Bonhoure J., Kister P., Cuney M. and Deloule E. (2007)
Methodology for rare earth element determinations of uranium oxides by ion microprobe. Geostandards and Geoanalytical Research, 31, 209–225.

Bürger S., Mathew K.J., Mason P. and Narayanan U. (2008)
Reference materials characterized for impurities in uranium matrices: An overview and re-evaluation of the NBL CRM 124 series. Journal of Radioanalytical and Nuclear Chemistry, 279, 659–673.

Bürger S., Boulyga S.F., Peńkin M.V., Bostick D., Jovanovic S., Lindvall R., Rasmussen G. and Riciputi L. (2014)
Quantifying multiple trace elements in uranium ore concentrates: An interlaboratory comparison. Journal of Radioanalytical and Nuclear Chemistry, 301, 711–729.

Dahlkamp F.J. (1991)
Uranium ore deposits. Springer (Berlin), 460pp.

Fryer B.J., Jackson S.E. and Longerich H.P. (1995)
The design, operation and role of the laser-ablation microprobe coupled with an inductively coupled plasma-mass spectrometer (LAM-ICP-MS) in the earth sciences. The Canadian Mineralogist, 33, 303–312.

George L.L., Cook N.J., Crowe B.B.P. and Ciobanu C.L. (2018)
Trace elements in hydrothermal chalcopyrite. Mineralogical Magazine, 82, 59–88.

Günther D. and Hattendorf B. (2005)
Solid sample analysis using laser ablation inductively coupled plasma mass spectrometry. Trends in Analytical Chemistry, 24, 255–265.

references

Hiess J., Condon D.J., McLean N. and Noble S.R. (2012)
$^{238}U/^{235}U$ systematics in terrestrial uranium-bearing minerals. Science, 335, 1610–1614.

Janeczek J. and Ewing R.C. (1992)
Structural formula of uraninite. Journal of Nuclear Materials, 190, 128–132.

Jenner G.A., Longerich H.P., Jackson S.E. and Fryer B.J. (1990)
ICP-MS – A powerful tool for high-precision trace-element analysis in earth sciences: Evidence from analysis of selected U.S.G.S. reference samples. Chemical Geology, 83, 133–148.

Keegan E., Richter S., Kelly I., Wong H., Gadd P., Kuehn H. and Alonso-Munoz A. (2008)
The provenance of Australian uranium ore concentrates by elemental and isotopic analysis. Applied Geochemistry, 23, 765–777.

Kish L. and Cuney M. (1981)
Uraninite-albite veins from Mistamisk Valley of the Labrador Trough, Quebec. Mineralogical Magazine, 44, 471–483.

Krachler M., Varga Z., Nicholl A., Wallenius M. and Mayer K. (2018)
Spatial distribution of uranium isotopes in solid nuclear materials using laser ablation multi-collector ICP-MS. Microchemical, 140, 24–30.

Kristo M.J., Gaffney A.M., Marks N., Knight K., Cassata W.S. and Hutcheon I.D. (2016)
Nuclear forensic science: Analysis of nuclear material out of regulatory control. Annual Review of Earth and Planetary Sciences, 44, 555–579.

McDonough W.F. and Sun S.S. (1995)
The composition of the earth. Chemical Geology, 120, 223–253.

Mercadier J., Cuney M., Lach P., Boiron M.C., Bonhoure J., Richard A., Leisen M. and Kister P. (2011)
Origin of uranium deposits revealed by their rare earth element signature. Terra Nova, 23, 264–269.

Moody K.J., Grant P.M. and Hutcheon I.D. (2015)
Nuclear forensic analysis (2nd edition). CRC Press (Boca Raton, USA), 502pp.

New Brunswick Laboratory (2010)
CRM 112-A, Uranium (normal) metal assay and isotopic standard. U.S. Department of Energy (Argonne, USA).

Pearce N.J.G., Perkins W.T., Westgate J.A., Gorton M.P., Jackson S.E., Neal C.R. and Chenery S.P. (1997)
A compilation of new and published major and trace element data for NIST SRM 610 and NIST SRM 612 glass reference materials. Geostandards Newsletter: The Journal of Geostandards and Geoanalysis, 21, 115–144.

Pollington A.D., Kinman W.S., Hanson S.K. and Steiner R.E. (2016)
Polyatomic interferences on high precision uranium isotope ratio measurements by MC-ICP-MS: Applications to environmental sampling for nuclear safeguards. Journal of Radioanalytical and Nuclear Chemistry, 307, 2109–2115.

Pouchou J. and Pichoir F. (1991)
Quantitative analysis of homogeneous or stratified microvolumes applying the model "PAP". In: Heinrich K.F.J. and Newbury D.E. (eds), Electron probe quantitation. Plenum (New York, USA), 31–75.

Schurr M.R., Donohue P.H., Simonetti A. and Dawson E.L. (2018)
Multi-element and lead isotope characterisation of early nineteenth century pottery sherds from Native American and Euro-American sites. Journal of Archaeological Science: Reports, 20, 390–399.

Spano T.L., Simonetti A., Balboni E., Dorais C. and Burns P.C. (2017)
Trace element and U isotope analysis of uraninite and ore concentrate: Applications for nuclear forensic investigations. Applied Geochemistry, 84, 277–285.

Trites A.F. and Chew R.T. (1955)
Geology of the Happy Jack mine White Canyon area San Juan County, Utah. In: A contribution to the geology of uranium. U.S. Department of the Interior Geological Survey Bulletin 1009-H, 235–248.

Varga Z., Katona R., Stefanka Z., Wallenius M., Mayer K. and Nicholl A. (2010)
Determination of rare-earth elements in uranium-bearing materials by inductively coupled plasma mass spectrometry. Talanta, 80, 1744–1749.

Supporting information

The following supporting information may be found in the online version of this article:

Appendix S1. Supplementary materials.

This material is available from: http://onlinelibrary.wiley.com/doi/10.1111/ggr.12293/abstract (This link will take you to the article abstract).